Available online at www.sciencedirect.com

ScienceDirect

Polyhedron 26 (2007) 3893–3903

POLYHEDRON

www.elsevier.com/locate/poly

Synthesis, characterization and structures of copper(II) complexes with amide-based ligands: Unusual formation of a linear trimer and a zig-zag chain and their contrast magnetic behaviour

Jyoti Singh [a], Geeta Hundal [b], Montserrat Corbella [c,*], Rajeev Gupta [a,*]

[a] *Department of Chemistry, University of Delhi, Delhi 110 007, India*
[b] *Department of Chemistry, Guru Nanak Dev University, Amritsar 143 005, Punjab, India*
[c] *Departament de Química Inorgànica, Universitat de Barcelona, Martí I Franquès 1-11, E-08028-Barcelona, Spain*

Received 9 March 2007; accepted 14 April 2007
Available online 30 April 2007

Abstract

The present work illustrates the versatile coordination modes of the amide-based ligands towards copper(II) ion. The reaction of the deprotonated form of the ligand, $[L^1]^{2-}$ with $CuCl_2$ affords a linear trinuclear complex, $[Cu_3(L^1)_2(Cl)_2(H_2O)]$ (**1**) which has been characterized thoroughly including single crystal structure analysis. The structure of **1** shows that one of the arm of the flexible ligand flips to coordinate second copper(II) centre, resulting in the formation of a trinuclear complex. On the other hand, ligand H_2L^2 in its deprotonated form reacts with Cu(II) ion to give complex **2** with general formula, $[Cu(L^2)]_n$ (**2**). The crystal structure of the complex **2** shows that each copper is square-pyramidal with 5th coordination coming from the O-atom of the amide group from a neighbouring complex. This results in the generation of an one-dimensional zig-zag chain. The variable temperature magnetic measurements of the complexes, **1** and **2** show that while Cu ions in the former are *antiferromagnetically* coupled ($J = -110.34\ \text{cm}^{-1}$), a weak *ferromagnetic* interaction ($J = +3.08\ \text{cm}^{-1}$) exists in the later. A rationale, based on the orbital overlap from the copper ions and associated ligands, is provided for the observed magnetic coupling between the copper ions.

Keywords: Copper(II) complexes; Amide ligands; X-ray structures; Magnetic properties

1. Introduction

Multinuclear metal clusters are ubiquitous to a number of biological systems. Particular interest in multi-copper complexes has been sparked in recent years by the characterization of several metalloenzymes that contain multi-copper centres [1–4], including particulate methane monooxygenase (pMMO) [5] and nitrous oxide reductase (NOR) [6]. The recently solved crystal structure of NOR shows the presence of a μ_4-sulfide bridged tetranuclear copper cluster [7–9]. Whereas, very recently, the crystal structure of pMMO reveals interesting sub-units having mononuclear and dinuclear copper centres [10]. The exact nature of the ligands present and their coordination mode is not clear due to the limitations of the 2.8 Å resolution of the crystal structure. In this context, appropriate synthetic model helps in better understanding to the elucidation of the active site structure [11].

Another reason of interest into multi-copper systems resides in the inherent magnetic interactions these systems offer. Numerous examples of magnetic interaction in exogenous ligand(s) bridged copper(II) binuclear and polynuclear complexes have been reported [12–14]. On the other hand, when the endogenous ligand(s) is involved in providing the bridge for the magnetic superexchange; examples are mainly limited to alkoxide- [15–17] and phenoxide-based [18–20] ligands. There are comparatively fewer examples when a endogenous ligand(s) capable of

---

* Corresponding authors. Tel.: +91 11 2766 7624; fax: +91 11 2766 6605 (R. Gupta).
E-mail address: rgupta@chemistry.du.ac.in (R. Gupta).

0277-5387/$ - see front matter © 2007 Elsevier Ltd. All rights reserved.
doi:10.1016/j.poly.2007.04.021

simultaneously coordinating two or more metal centers also provide the bridge for the magnetic interaction; especially when the metal ions are relatively far from each other. In this category, $X_2C_2Y_2$ bridge, where X and Y atoms bound to different metal ions may be O, N, or S, has been used efficiently to propagate the magnetic interactions between two and in very few cases three metal centers. The examples include highly symmetrical bridge oxalato, $O_2C_2O_2^{2-}$ [21–23], oxamido, $N_2C_2O_2^{2-}$ [24–27], and dithiooxamido, $N_2C_2S_2^{2-}$ [28–30]. In particular, the oxamido ligand provide two planar NCO bridge between the metal centres and the result is a very strong antiferromagnetic coupling [24–27].

In this paper, we describe the design and synthesis of two amide-based ligands and their copper coordination chemistry. The ligands coordinate the copper ion via deprotonated $N_{amidate}$ and neutral N_{amine} donors. Interestingly, in one case, flipping of the amide containing arm take place to afford a linear copper trinuclear complex. This is a rare example, where deprotonated amide group coordinate via both ends, $N_{amidate}$ as well as $O_{amidate}$ [31,32]. The second complex also shows sharing of the amide group between copper centres affording a one-dimensional zig-zag chain. The bridging ligand present between the copper(II) ions is NCO, thus we have chopped off one unit (one NCO fragment) of the oxamido ligand. The result of this alteration on the structure and magnetic properties of the copper complexes is presented.

2. Experimental

2.1. Materials

All reagents were obtained from the commercial sources and used as received. *N*,*N*-dimethyl formamide (DMF) was dried and distilled from 4 Å molecular sieves and was stored over sieves. Acetonitrile (MeCN) was dried by distillation from anhydrous CaH_2. Diethyl ether and petroleum ether (boiling range 60–80 °C) were dried by refluxing over sodium metal under inert atmosphere. Tetrahydrofuran (THF) was dried by refluxing and distilling from sodium metal and benzophenone. Ethyl alcohol (C_2H_5OH) and methyl alcohol (CH_3OH) were distilled from magnesium ethoxide and magnesium methoxide, respectively. Chloroform ($CHCl_3$) and dichloromethane (CH_2Cl_2) were purified by washing with 5% sodium carbonate solution followed by water and finally dried over anhydrous $CaCl_2$, before a final reflux and distillation. *N*,*N*′-bis(chloroacetyl)ethylenediamine and *N*,*N*′-bis(chloroacetyl)-*o*-phenylenediamine were synthesized according to a reported procedure [33,34].

2.2. Physical measurements

The conductivity measurements were done in organic solvents using the digital conductivity bridge from Popular Traders, India (model number: PT-825). The elemental analysis data were obtained from Elementar Analysensysteme GmbH Vario EL-III instrument. The NMR measurements were done using an Avance Bruker (300 MHz) instrument. The infra-red spectra (either as KBr pellet or as a mull in mineral oil) were recorded using the Perkin–Elmer FTIR 2000 spectrometer. The absorption spectra were recorded using the Perkin–Elmer Lambda-25 spectrophotometer. The mass spectra were obtained on a Jeol SX102/DA-6000 instrument. The thermal analyses were performed with a Shimadzu DTG-60 instrument in the temperature range of 25–800 °C. EPR spectra of the polycrystalline samples were recorded at X-band (9.4 GHz) frequencies with a Bruker ESP-300E spectrometer, from room temperature to 4 K at the Servei de Magnetoquimica of the Universitat de Barcelona. Room temperature solution EPR spectra were recorded with a Jeol JES-3XG spectrometer.

2.3. Crystallography

Single crystals suitable for X-ray diffraction studies were grown by the vapour diffusion of diethyl ether to a DMF solution of complex **1** and slow evaporation of a saturated MeOH solution of **2**. The suitable crystals of **1** and **2** were mounted lengthways with the largest dimension in a sealed capillary. The intensity data for **1** were collected at 295 K on a Siemens P4 X-ray diffractometer by using scanning mode with graphite monochromatized Mo Kα radiation. A total of 15503 reflections were measured of which 10999 reflections ($I > 2\sigma(I)$) were used in the structure refinement. The data were corrected for Lorentz and polarization effects and a psi-scan absorption correction was also applied. The structure was solved by direct methods and refined by full-matrix least-squares refinement techniques on F^2. There are two crystallographically independent molecules of the complex and the solvent DMF in the unit cell. All calculations were performed using SHELXTL-PC. One of the DMF molecules showed rotational disorder which has been treated by refining all five non-hydrogen atoms of this molecule (C60, C61, C62, N20, O12) being split at two sites with total site occupancy of 1.00 for each one of them. This DMF molecule was refined isotropically with similar U_{iso} values assigned to two atoms of the pair. The molecule was refined with restraints on the bond distances of this disordered molecule being $C(sp^3)$–N 1.440(3), $C(sp^2)$–N 1.350(3), C=O 1.226(3) Å and non-bonding distances being 2.20(3) Å. All non-hydrogen atoms except for one DMF molecule were refined anisotropically. All hydrogen atoms were attached geometrically except for those belonging to the water molecules which were determined from the difference Fourier map. For **2**, the intensity data were collected on a BRUKER AXS SMART-APEX CCD diffractometer equipped with a molybdenum sealed tube (Mo Kα = 0.71073 Å) and a highly orientated graphite monochromator [35]. Frames were collected at $T = 293$ K by ω, ϕ and 2θ-rotation at 10 s per frame with SMART [35]. The measured intensities were reduced to F^2 and corrected for absorption with

SADABS [36]. The structure of **2** was solved by SIR 92 expanded by Fourier difference syntheses and refined with the SHELXL 97 package incorporated in WINGX 1.64 crystallographic collective package [37–39]. The positions of the hydrogen atoms were calculated by assuming ideal geometries but not refined. All non-hydrogen atoms were refined with anisotropic thermal parameters by full-matrix least-squares procedures on F^2. Details of the crystallographic data are given in Table 1.

2.4. Magnetic measurements

Magnetic susceptibility measurements for crushed crystalline samples of **1** and **2** were carried out at the Servei de Magnetoquimica of the Universitat de Barcelona with a Quantum Design SQUID MPMS-XL susceptometer. The magnetic susceptibility data were recorded in the 2–300 K temperature range under magnetic fields of 500 G (2–30 K) and 10000 G (2–300 K). Diamagnetic corrections were estimated from Pascal Tables. The fits were performed minimizing the function $R = \Sigma(\chi_M T_{\mathrm{exp}} - \chi_M T_{\mathrm{cal}})^2/\Sigma(\chi_M T_{\mathrm{exp}})^2$. Magnetic fields ranging from 0 to 50000 G were used for magnetization measurements at 2 K.

2.5. Ligand Syntheses

2.5.1. Synthesis of H_2L^1

To a solution of diethylamine (1.37 g, 18.76 mmol) in MeCN (30 cm^3), K_2CO_3 (39 g, 282 mmol) and *N*,*N*′-bis(chloroacetyl)ethylenediamine (2 g, 9.38 mmol) were added and the mixture was refluxed for 24 h. The mixture was cooled, filtered and the solvent was removed under reduced pressure to afford an off-white solid. The crude product was recrystallized by layering the $CHCl_3$ solution with the petroleum ether (boiling range 60–80 °C). Yield: 2.24 g, 83%. Microanal. Calc. for H_2L^1, $C_{14}H_{30}N_4O_2$: C, 58.74; H, 10.57; N, 19.58. Found: C, 58.28; H, 10.96; N, 19.52%. M.p. 80 °C. Selected IR bands (FT-IR, KBr) ν (cm^{-1}): 3301s (NH), 2965m, 2933m, 2873w, 2814w (CH), 1649s (C═O). ^{1}H NMR spectrum ($CDCl_3$): δ 1.023 (t, $J = 6.8$ Hz, 12H, ethyl CH_3), 2.54 (quartet, $J = 6.7$ Hz, 8H, ethyl CH_2), 3.01 (s, 4H, CH_2CO), 3.42 (s, 4H, ethylene CH_2), 7.65 (br s, 2H, amidic NH). ESI mass spectrum (CH_3CN): $m/z = 287.24$ [M+H$^+$].

Table 1
Crystallographic data for complexes, $[Cu_3(L^1)_2(Cl)_2(H_2O)] \cdot DMF$ (**1**) and $[Cu(L^2)]_n$ (**2**)

	1 · DMF	**2**
Formula	$C_{31}H_{65}N_9O_6Cl_2Cu_3$	$C_{14}H_{20}N_4O_2Cu$
M_r	921.47	339.88
Crystal system	triclinic	orthorhombic
Space group	$P\bar{1}$ (#2)	$Pn21a$ (#33)
a (Å)	13.078(5)	16.560(5)
b (Å)	17.696(5)	8.427(5)
c (Å)	21.210(5)	11.203(5)
α (°)	102.420(5)	90.0
β (°)	93.680(5)	90.0
γ (°)	110.500(5)	90.0
V (Å^3)	4438(2)	1563.4(13)
Z	4	4
T (K)	295(2)	293(2)
Colour, shape	blue, prism	blue, block
Crystal size (mm)	0.18 × 0.15 × 0.13	0.3 × 0.2 × 0.2
D_{calc} (g cm^{-3})	1.379	1.444
$F(000)$	1932	708
R^{a}	0.0598	0.0450
wR^{b}	0.1683	0.1171
Goodness of fit on F^2	1.031	0.831
$\Delta\rho_{\mathrm{max,min}}$ (e Å^{-3})	0.710, −1.184	0.351, −0.560

[a] $R = \sum||F_o| - |F_c||/\sum|F_o|$.
[b] $wR = \{[\sum(|F_o|^2|F_c|^2)^2]\}^{1/2}$.

2.5.2. Synthesis of H_2L^2

To a solution of *N*,*N*′-bis(chloroacetyl)-*o*-phenylenediamine (2 g, 7.6 mmol) in ethanol (25 cm^3), 40% aqueous solution of dimethylamine (5.2 g, 46 mmol) was added and the mixture was refluxed for 24 h. The mixture was cooled and the solvent was removed under reduced pressure. The resultant oil was washed with a saturated solution of $NaHCO_3$ (10 cm^3) and the ligand was then extracted with dichloromethane (3 × 10 cm^3). The combined extracts were dried over Na_2SO_4 and evaporated under reduced pressure to leave a pale yellow solid. The crude product was then recrystallized by layering the $CHCl_3$ solution with the petroleum ether (boiling range 60–80 °C). Yield: 1.8 g, 85%. Microanal. Calc. for H_2L^2, $C_{14}H_{22}N_4O_2$: C, 60.31; H, 7.8; N, 20.10. Found: C, 59.59; H, 7.6; N, 19.86%. M.p. 82 °C. Selected IR bands (FT-IR, KBr) ν (cm^{-1}): 3231m (NH), 2952w, 2826m, 2780m (CH), 1693s (C═O), 1601m (C═C). ^{1}H NMR spectrum ($CDCl_3$): δ 2.30 (s, 12H, methyl CH_3), 3.03 (s, 4H, CH_2CO), 7.10 (m, 2H, benzyl CH) 7.56 (m, 2H, benzyl CH), 9.17 (br s, 2H, amidic NH). ESI mass spectrum (CH_3CN): $m/z = 279.4$ [M+H$^+$].

2.6. Syntheses of the copper complexes

2.6.1. $[Cu_3(L^1)_2(Cl)_2(H_2O)] \cdot 2H_2O$ (**1**)

To a stirred solution of H_2L^1 (0.200 g, 0.699 mmol) in DMF (10 cm^3), solid NaH (0.033 g, 1.398 mmol) was added under dinitrogen atmosphere. The resulting mixture was stirred until H_2 evolution ceased. To this $CuCl_2$ (0.141 g, 1.048 mmol) was added as solid followed by the addition of few drops of water. The resulting green-blue solution was stirred at room temperature for 2 h. During this time the colour changed to dark blue. The solution was passed through a celite pad in a medium porosity frit. The resultant solution was layered with diethyl ether and stored at 4 °C. This afforded dark blue microcrystalline product within a day. Yield: 0.18 g, 61%. Microanal. Calc. for **1**, $C_{28}H_{58}N_8O_5Cl_2Cu_3 \cdot 2H_2O$: C, 38.03; H, 7.01; N, 12.68. Found: C, 38.36; H, 7.20; N, 12.56%. Selected IR bands (FT-IR, KBr) ν (cm^{-1}): 3367m br. (OH), 2967m, 2930m, 2874m (CH), 1610s, 1572s (C═O). UV–Vis spectrum (MeCN: λ_{max} (nm) [ε_{max}] (M^{-1} cm^{-1})): 625 [390], 515sh [280], 350sh [4230], 317sh [7700], 264 [14050]. UV–Vis spectrum (MeOH: λ_{max} (nm) [ε_{max}] (M^{-1} cm^{-1})): 625 [370], 260 [15200], 215 [27800]. Conductivity (CH_3CN, ~1 mM solution, 298 K): $\Lambda_M = 12\ \Omega^{-1}\ cm^2\ mol^{-1}$. ESI mass spectrum ($CH_3OH$) $m/z = 852.5$ ($[Cu_3(L^1)_2(CH_3OH)(OCH_3)_2]+H^+$).

2.6.2. $[Cu(L^2)]_n$ (**2**)

To a stirred solution of H_2L^2 (0.200 g, 0.719 mmol) in DMF (10 cm^3), solid NaH (0.034 g, 1.438 mmol) was added under dinitrogen atmosphere. The resulting solution was stirred until H_2 evolution ceased. Solid $CuCl_2$ (0.097 g, 0.719 mmol) was added to the above mixture. The resulting indigo-blue solution was stirred at room temperature for 2 h. The DMF was then removed under reduced pressure and the residue was redissolved in CH_3OH (50 cm^3). The solution was passed through the celite pad in a medium porosity frit and allowed to evaporate for a day to afford dark blue microcrystalline product. The product was filtered and dried under vacuum. Yield: 0.20 g, 82%. Microanal. Calc. for **2**, $C_{14}H_{20}N_4O_2Cu$: C, 49.33; H, 5.89; N, 16.49. Found: C, 49.33; H, 6.03; N, 16.33%. Selected IR bands (FT-IR, KBr) ν (cm^{-1}): 3060w, 2893w, 2793w (CH), 1616s, 1598s (C=O), 1564s, 1478m, 1454w (C=C). UV–Vis spectrum (MeOH: λ_{max} (nm) [ε_{max}] (M^{-1} cm^{-1})): 550 [410], 413sh [180], 311sh [12270], 302sh [18600], 270 [47050], 250sh [52500], 240 [62050]. UV–Vis spectrum (MeCN: λ_{max} (nm) [ε_{max}] (M^{-1} cm^{-1})): 530 [360], 405sh [175], 311sh [11050], 280 [31000], 242 [50400], 214 [28000]. conductivity (CH_3OH, ~1 mM solution, 298 K): $\Lambda_M = 16\ \Omega^{-1}\ cm^2\ mol^{-1}$. ESI mass spectrum ($CH_3OH$) $m/z = 362.18$ ($[Cu(L^2)]+Na^+$).

3. Results and discussion

3.1. Ligand design and synthesis

The ligands H_2L^1 and H_2L^2 are designed to simultaneously provide two amide and two amine coordinations to the metal centre while maintaining an identical primary coordination environment around it. While the ligand H_2L^1 has a flexible ethylenediamine backbone, the ligand H_2L^2 incorporates a rigid *o*-phenylenediamine backbone. These ligands are synthesized in two steps starting from the corresponding primary diamines. In the first step, the diamine is converted to the respective bis(chloroamide) by treating with 2 equiv. of chloroacetyl chloride [33,34]. In the second step, the bis(chloroamide) was subsequently treated with diethyl- or dimethyl-amine to afford the ligands, H_2L^1 and H_2L^2, respectively. Excess Me_2NH (6 equiv.) was used for the synthesis of H_2L^2, where it also functioned as a base in the reaction. Both ligands were characterized thoroughly and gave satisfactory microanalyses results.

3.2. Synthesis and characterization of copper complexes

Complex **1** was synthesized by the initial reaction of 2 equiv. of deprotonated ligands with 3 equiv. of $CuCl_2$. The reaction mixture was then treated with few drops of water to afford the final compound (Scheme 1). The complex **2** was also synthesized in an analogous fashion by treating deprotonated ligand, $[L^2]^{2-}$, with $CuCl_2$ (Scheme 2). In the FTIR spectra, the absence of ν(N–H) stretching frequency confirms the deprotonated nature of the amide ligands. Moreover, a *red* shift was observed for the amidate C=O group compared to the free ligand, thus indicating coordination through anionic amidate-N center. The complex **1** also shows the ν(OH) stretches in the region of ~3370 cm^{-1} for the coordinated as well as lattice water [40]. Solution conductivity data [41] confirms the non-electrolytic nature of both copper complexes, whereas elemental analyses results authenticate the purity of the bulk samples. In the electrospray mass spectrum for complex **1** in CH_3CN, the molecular ion peak was observed at 887.35 that matches well with the following composition, $[Cu_3(L^1)_2(Cl)_2(H_2O)] + H_2O + Na^+$ (calculated $m/z = 887.64$). This is to be noted, however, when recorded in CH_3OH, a new molecular ion peak was observed at 852.5 which fits well with the following composition,

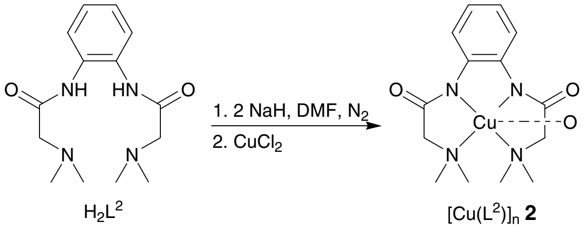

Scheme 2. Synthesis of complex **2**.

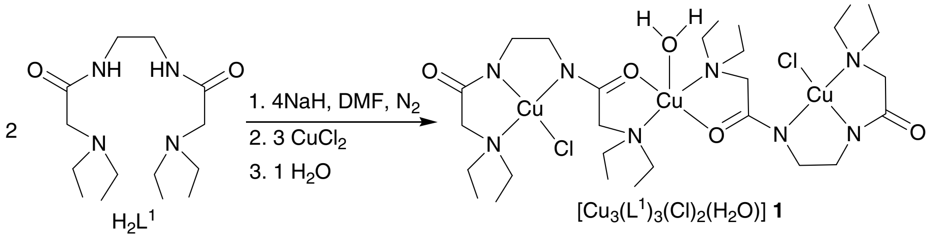

Scheme 1. Synthesis of complex **1**.

$[Cu_3(L^1)_2(OCH_3)_2(CH_3OH)] + H^+$ (calculated $m/z = 852.3$). Interestingly, while recording the spectrum in CH_3OH, two chloride ions were replaced by methoxide ions while the coordinated water got exchanged with methanol. Complex **2**, on the other hand, shows the molecular ion peak at 362.18 that matches well with $[Cu(L^2)] + Na^+$ (calculated $m/z = 362.25$).

3.3. Solid state structures

*3.3.1. Structure of complex **1***

The molecular structure of **1** contains two slightly different independent trinuclear motifs of $[Cu_3(L^1)_2(Cl)_2(H_2O)]$, hereafter referred as molecule A and molecule B. The thermal ellipsoidal representation of molecules A and B are shown in Fig. 1 while important structural parameters are presented in Table 2. Each trinuclear assembly is composed of two $[L^1]^{2-}$ ligands, three copper ions, two chloride ions, and a water molecule. The terminal copper ions (Cu1 and Cu3 in molecule A; and Cu4 and Cu6 in molecule B) are coordinated by two amidate-N centres, one amine-N centre, and a chloride ion completing a distorted square-planar geometry. The central copper ion (Cu2 and Cu5 in molecules A and B, respectively) is coordinated by two amine-N centres, two amidate-O centres, and an apical water molecule. The geometry around the central copper(II) ion is distorted square-pyramidal. The τ value [42], which is an indication of the distortion of the 5-coordinate geometry towards square-pyramidal ($\tau = 0$) or trigonal bipyramidal ($\tau = 1$), is 0.14 and 0.04, for central copper ion in molecules A and B, respectively. It is clear from the value of τ that the central Cu(II) ion has much more distorted geometry in molecule A. The displacement from the basal plane (defined by two amide-N, one amine-N, and a Cl^-) for the terminal copper centres (Cu1, Cu3, Cu4, and Cu6) is quite small, 0.028–0.087 Å. On the other hand, the central coppers are significantly displaced out of basal plane (defined by two amide-Os and two amine-Ns) towards the apical water molecule; displacement for Cu2 and Cu5 is 0.210 and 0.171 Å, respectively. These values again indicate that the copper ion in molecule A has much more distorted geometry than in B. The bond length difference for the coordination of two amidate-N centres to the terminal Cu(II) ions (for example, between Cu1–N2 and Cu1–N3 for molecule A) is quite significant, ~0.1 Å. This difference may be attributed due to the presence of a delocalized structure of one of the amide group which is involved in the bonding with the central Cu(II) ion. This

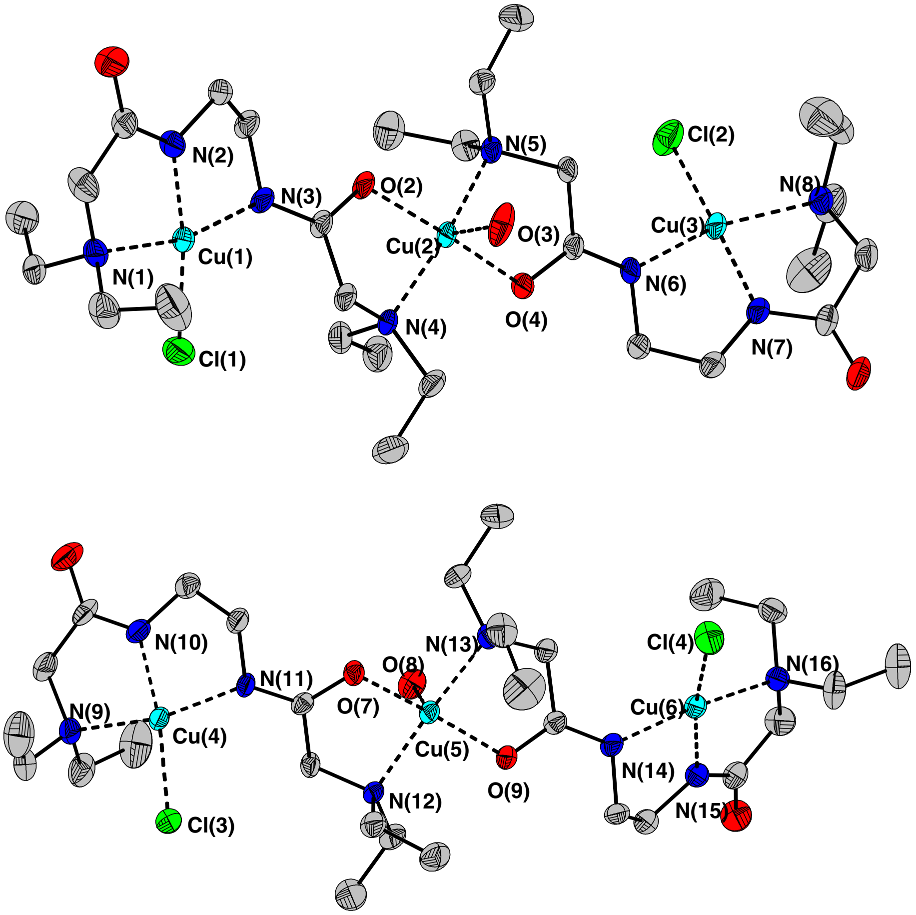

Fig. 1. Thermal ellipsoidal representation (30% probability level with partial numbering) of complex **1** (molecule **A** (top) and molecule **B** (bottom) Hydrogen atoms and solvent molecules are omitted for clarity.

Table 2
Selected bond distances (Å) and angles (°) for molecules A and B in complex $[Cu_3(L^1)_2(Cl)_2(H_2O)]$ (**1**)

Molecule A		Molecule B	
Bond distances			
Cu1–N1	2.105(4)	Cu4–N9	2.083(4)
Cu1–N2	1.898(4)	Cu4–N10	1.891(4)
Cu1–N3	2.007(4)	Cu4–N11	1.993(4)
Cu1–Cl1	2.2226(19)	Cu4–Cl3	2.2393(17)
Cu2–N4	2.051(4)	Cu5–N12	2.057(4)
Cu2–N5	2.045(4)	Cu5–N13	2.043(4)
Cu2–O2	1.938(3)	Cu5–O7	1.938(3)
Cu2–O3	2.192(4)	Cu5–O8	2.271(4)
Cu2–O4	1.942(3)	Cu5–O9	1.923(3)
Cu3–N6	1.981(4)	Cu6–N14	2.001(4)
Cu3–N7	1.894(4)	Cu6–N15	1.894(4)
Cu3–N8	2.109(4)	Cu6–N16	2.117(4)
Cu3–Cl2	2.2332(19)	Cu6–Cl4	2.2251(18)
Bond angles			
N2–Cu1–N3	83.04(17)	N10–Cu4–N11	83.00(19)
N2–Cu1–N1	81.98(18)	N10–Cu4–N9	83.4(2)
N3–Cu1–N1	164.89(18)	N11–Cu4–N9	161.3(2)
N2–Cu1–Cl1	171.24(15)	N10–Cu4–Cl3	166.18(17)
N3–Cu1–Cl1	102.56(14)	N11–Cu4–Cl3	102.02(13)
N1–Cu1–Cl1	92.10(14)	N9–Cu4–Cl3	94.16(15)
O4–Cu2–O2	172.18(17)	O9–Cu5–O7	168.71(17)
O4–Cu2–N5	83.30(15)	O9–Cu5–N13	84.75(16)
O2–Cu2–N5	96.03(15)	O7–Cu5–N13	95.75(16)
O4–Cu2–N4	95.42(15)	O9–Cu5–N12	94.02(15)
O2–Cu2–N4	83.07(15)	O7–Cu5–N12	83.69(15)
N5–Cu2–N4	164.00(18)	N13–Cu5–N12	170.85(19)
O4–Cu2–O3	94.08(16)	O9–Cu5–O8	93.97(16)
O2–Cu2–O3	93.73(16)	O7–Cu5–O8	97.26(16)
N5–Cu2–O3	97.54(19)	N13–Cu5–O8	93.18(18)
N4–Cu2–O3	98.5(2)	N12–Cu5–O8	95.95(17)
N7–Cu3–N6	82.35(18)	N15–Cu6–N14	82.76(19)
N7–Cu3–N8	82.55(18)	N15–Cu6–N16	81.80(18)
N6–Cu3–N8	164.07(19)	N14–Cu6–N16	162.59(19)
N7–Cu3–Cl2	166.77(16)	N15–Cu6–Cl4	167.67(16)
N6–Cu3–Cl2	100.61(14)	N14–Cu6–Cl4	100.66(14)
N8–Cu3–Cl2	95.24(14)	N16–Cu6–Cl4	96.12(14)
Cu1–Cu2–Cu3	176.61(11)	Cu4–Cu5–Cu6	170.139(12)

delocalization of the electron density has contributed in inducing a partial negative charge on the amidate-O atom that eventually coordinate to the central copper ion to afford the linear trinuclear complex. The implication of this delocalized resonance structure is the lengthening of the C=O bond involved in the bonding than the un-coordinated one. The C=O bond length increased from a average value of ~1.23(2) Å (uncoordinated one) to ~1.28(2) Å (coordinated one). This lengthening is lower for molecule B (0.03–0.04 Å) than for molecule A (0.05–0.06 Å). The $Cu–O_{amide}$ distances for the central metal ion, are in the range of 1.923(3)–1.942(3) Å for molecules A and B. These distances are on the lower side than the examples reported in the literature and indicate a stronger bond to the copper ion [31,32]. The $Cu–OH_2$ bond distances are also on the lower side compared to the similar distance in other structurally characterized complexes [43–47]. The Cu–Cl distances are comparable to other structurally characterized complexes [48–50]. The average distance between the neighbouring copper centres is ~5.74(3) Å, while the terminal copper ions are separated by ~11.5(3) Å. The coordinated water molecule forms hydrogen bonds with the carbonyl oxygen atoms from the neighbouring complexes, the distance are within the range of ~2.62(3)–2.68(4) Å.

There are strong H-bonding interactions involving the amide oxygens, water molecules and the DMF molecule resulting in an interesting crystal structure of the molecule. The water molecule O3 of molecule A shows strong intermolecular O···O bonding with amide oxygens O1 and O5 of its centrosymmetrically related molecules (Table S1). This gives rise to polymeric, pleated ribbon like chains running along the *c* axis in the *bc* plane (Fig. S1) constituting lattice I. The DMF molecule close to this is not involved in any O···O bonding but is merely being held in space by weak C···O H-bonding interactions. On the other hand second DMF molecule is acting as H-bond acceptor to water molecule O8 of molecule B, which is also behaving as a H-bond donor to amide oxygen O10. These interactions give rise to a H-bonded 2B:2DMF tetrameric synthon as shown in Fig. S2, constituting lattice II. There are only some weak C···O H-bonding interactions between these synthons. Thus involvement of DMF in H-bonding interactions with the trinuclear coordination compound destroys the polymeric nature of molecule B. Taken together the crystal structure may be looked at as two interpenetrating lattices I and II (Fig. S3).

The alignment of the basal plane containing metal centers plays a very important role in the magnetic exchange interactions in any multimetallic system [51,52]. If these planes are coplanar with each other, a strong antiferromagnetism results and deviation from this planarity results in the alteration of the extent of orbital overlapping. The angle between the basal planes containing copper ion is within the range of 20–40°. For example, in molecule B, the angle between the planes containing Cu(4) and Cu(5) is 39.61°. These numbers suggest a moderate to weak antiferromagnetic interaction between the magnetic orbitals emerging from the planes containing copper ions (cf. magnetic properties).

3.3.2. *Structure of complex* **2**

The molecular structure of this complex is shown in Fig. 2 and the selected bonding parameters are presented in Table 3. The complex **2** exists as a one-dimensional (1D) chain of infinite length. The copper(II) ion is coordinated by the ligand $[L^1]^{2-}$, in a tetradentate fashion via two deprotonated amidate-N and two amine-N centers. The 5th coordination comes from the oxygen atom of the amide group of the neighbouring complex, with the distance of 2.354(2) Å. This additional interaction leads to the generation of an infinite length chain in the solid state. The geometry around the Cu(II) ion is almost perfect square – pyramidal with a very small τ value [42] of 0.01. The average $Cu–N_{amide}$ distance at 1.935(2) Å is shorter by 0.14 Å than the average $Cu–N_{amine}$ bond lengths of 2.075(3) Å, thus indicating a tight chelation from the

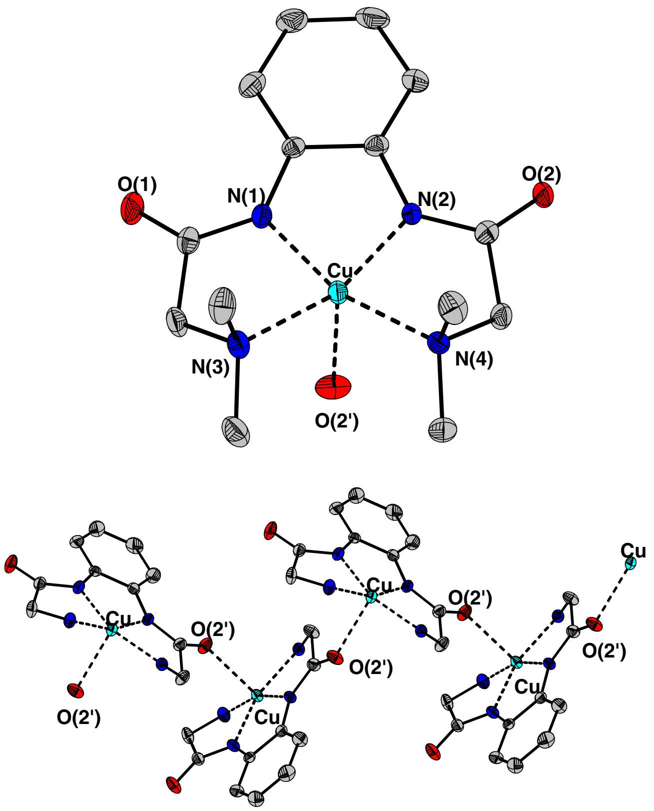

Fig. 2. Thermal ellipsoidal representation (30% probability level with partial numbering, hydrogen atoms are omitted for clarity) of complex **2**. Top: monomeric unit; bottom: zig-zag chain formation (methyl substituents are removed for clarity).

Table 3
Selected bond distances (Å) and angles (°) for complex $[Cu(L^2)]_n$ (**2**)

Bond distances			
Cu–N1	1.930(2)	C14–O1	1.232(4)
Cu–N2	1.939(2)	C7–O2	1.238(4)
Cu–N3	2.060(3)	N1–C14	1.321(4)
Cu–N4	2.090(3)	N2–C7	1.316(4)
Cu–O2′	2.354(2)		
Bond angles			
N1–Cu–N2	82.47(10)	N1–Cu–O2′	101.98(11)
N1–Cu–N3	162.19(11)	N2–Cu–O2′	104.48(10)
N2–Cu–N3	82.61(11)	N3–Cu–O2′	91.14(10)
N1–Cu–N4	82.29(11)	N4–Cu–O2′	88.91(11)
N2–Cu–N4	161.50(10)		
N3–Cu–N4	110.27(10)		

anionic amidate donors. The lateral 5-membered chelate rings are making an angle of ∼13° with each other, while they make an angle of 8–10° with the central 5-membered chelate ring. The copper(II) ion is 0.202 Å out of the least square basal plane (defined by N1, N2, N3, and N4) towards the apical amide oxygen atom from the neighbouring molecule. Any of the two copper ions in the chain are separated by ∼6 Å. The two neighbouring molecular planes containing copper ions make an angle of ∼74(1)° with each other. This significant number suggests that any of the two monomeric units in the 1D chain are almost orthogonal to each other and gave us a clue about their expected magnetic behaviour (cf. magnetic properties).

Vagg and co-workers [53] have reported a copper(II) complex with a pyridine-amide based ligand (*N*,*N*′-bis-(6′-methylpyridine-2′-carboxamide)-1,2-benzene) where oxygen atoms of the neighbouring molecules coordinate to form a chain. However, this is to be noted that here two O-atoms from two neighbouring molecules coordinate to complete an octahedral geometry around the copper ion. The two Cu–O_{amide} bond distances are 2.693(6) and 2.798(6) Å, respectively, and are quite longer than that of **2**. The average Cu–N_{amide} and Cu–$N_{pyridine}$ distances are 1.934(7) and 2.079(7) Å, respectively, and are quite similar to that of complex **2**. Interestingly, when the authors used the un-substituted pyridine-amide ligand (*N*,*N*′-bis(2′-pyridinecarboxamide)-1,2-benzene), only one water molecule coordinate axially to afford a square-pyramidal copper complex [54]. The authors have reasoned that the presence of methyl substituents on the pyridine ring in the former case caused the distortion around the metal centre and resulted in the twisting of the basal plane. The implication of this twisting is the availability of the coordination sites both from top and bottom of the basal plane, thus O_{amide} coordinate to the copper ion affording the octahedral geometry in the former case. Despite an interesting chain structure of the Cu(II) complex of Vagg and co-workers, magnetic properties have not been carried out.

3.4. Magnetic properties

The magnetic properties of **1** and **2** in the form of $\chi_M T$ versus T plot are shown in Figs. 3 and 4. For **1**, the value of $\chi_M T$, at room temperature is 1.13 $cm^3\,mol^{-1}\,K$, close to the expected value for three uncoupled Cu(II) ions. The $\chi_M T$ product decreases upon cooling, reaching a plateau at 23 K, with $\chi_M T$ value equal to 0.4 $cm^3\,mol^{-1}$. This value is close to the expected value for a spin state $S = 1/2$. This behaviour is characteristic of an antiferromagnetic

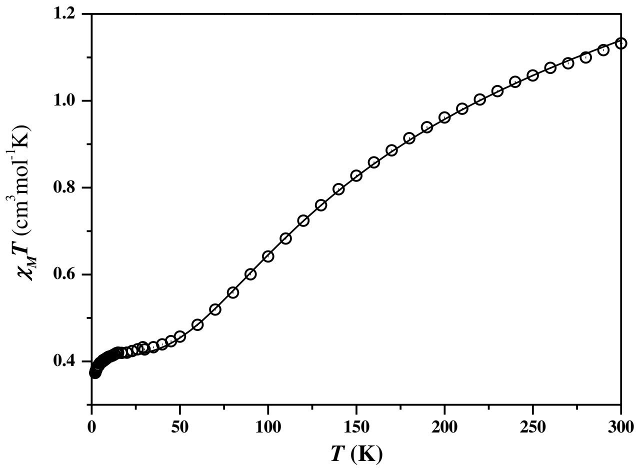

Fig. 3. $\chi_M T$ vs. T plot for compound **1**. The solid line was calculated with the parameters reported in the text.

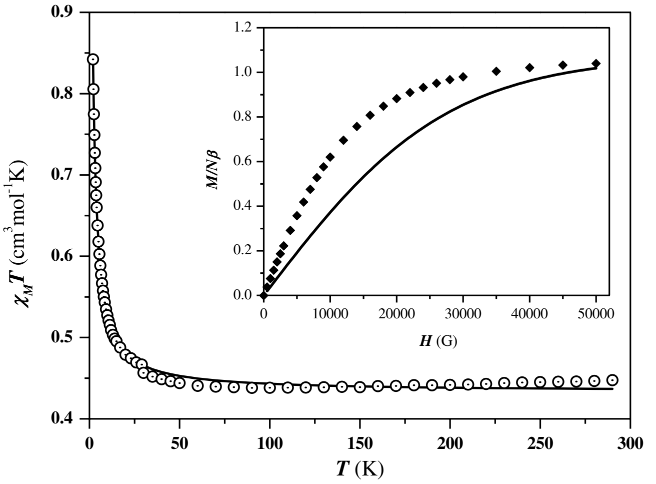

Fig. 4. $\chi_M T$ vs. T plot for compound **2**. The solid line was calculated with the parameters reported in the text. In the inset, experimental $M/N\beta$ vs. H plot (♦) and calculated from the brillouin equation for a $S = 1/2$ (solid line).

coupling. Below 4 K, $\chi_M T$ product decreases again, indicating that an intermolecular antiferromagnetic interaction also occur in this compound.

The experimental data were fitted using the theoretical expression deduced from the following Heisenberg Hamiltonian $H = -J(S_1 \cdot S_2 + S_2 \cdot S_3) - J'(S_1 \cdot S_3)$. Taking into account the geometry of this compound (the terminal copper centres are separated by the distance in the range of 11.4–11.5 Å), the interaction between the two terminal Cu(II) ions was assumed to be nil ($J' = 0$). The best fit was obtained for $J = -110.34\ \text{cm}^{-1}$ and $g = 2.06$ ($R = 1.8 \times 10^{-4}$).

For **2**, the $\chi_M T$ value at room temperature is $0.45\ \text{cm}^3\ \text{mol}^{-1}\ \text{K}$, which is as expected for one magnetically quasi-isolated Cu(II) ion ($g > 2.0$). On cooling, the $\chi_M T$ values smoothly increases up to $0.84\ \text{cm}^3\ \text{mol}^{-1}\ \text{K}$ at 2 K. The shape of this curve clearly indicates weak ferromagnetic coupling among the Cu(II) ions. The mathematical formula derived by Baker et al. [55] for ferromagnetic 1D systems with $S = 1/2$ is valid only at relatively high temperatures. Thus, when the ferromagnetic coupling is weak, this formula is not very accurate. For this reason, the fit of the experimental data was performed in the numerical form from a full-matrix diagonalization of the Hamiltonian corresponding to a ring of 12 local $S = 1/2$ centers with the adequate J coupling parameter using the CLUMAG program [56]. With this program, the use of 12 cycled centers give a good approximation for the system, which is actually infinite. The best fit parameters of the data are $J = +3.08\ \text{cm}^{-1}$ and $g = 2.15\ \text{cm}^{-1}$ ($R = 8.6 \times 10^{-5}$). The reduced molar magnetization ($M/N\beta$) per Cu entity tends to be 1 $N\beta$ (electron) (Fig. 4 inset) but the shape of the experimental curve is clearly above the theoretical ones for the Brillouin law. These features agree with the global ferromagnetic coupling between the copper(II) ions.

Compounds **1** and **2** show the same bridging motif, NCO, between the Cu(II) ions, nevertheless the magnetic behaviour is very different. For the trinuclear complex (compound **1**) strong antiferromagnetic coupling is observed, while the one-dimensional system (compound **2**) shows a ferromagnetic interaction.

In the trinuclear compound, the coordination around the two terminal ions is square planar, while for the central ion is a square pyramidal, and its basal plane is quite coplanar with the coordination planes of the terminal ions. For the three copper(II) ions, the single electron is in the $x^2 - y^2$ orbital, and taking into consideration that these orbitals are almost coplanars, a good overlap through the bridging motif NCO could be attended (Fig. 5). In the one-dimensional system, the coordination polyhedra of the Cu(II) ion is a square pyramidal, but, in this case, the basal planes between neighbours ions are almost perpendicular (in the crystal structure, two planes make an angle of 74° with each other), and as a result of this, the $x^2 - y^2$ orbital are orthogonal, and a very small overlap through the bridge must be attended (Fig. 6). So, the different magnetic behaviour observed for compounds **1** and **2**, could be explained by the different disposition of the magnetic orbitals.

Several trinuclear compounds with oxamide bridging ligands have been reported in the literature [24–30]. These trinuclear compounds show significant antiferromagnetic coupling with the J value ranging between −80 and

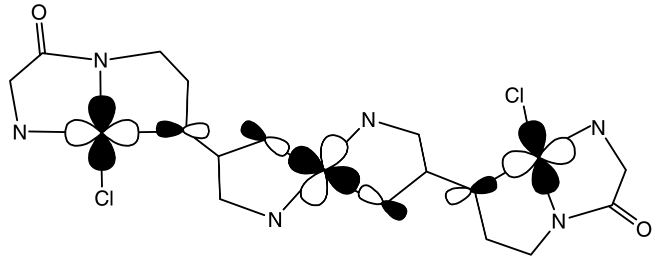

Fig. 5. Schematic drawing of the disposition of the $x^2 - y^2$ orbital in the trinuclear compound **1**.

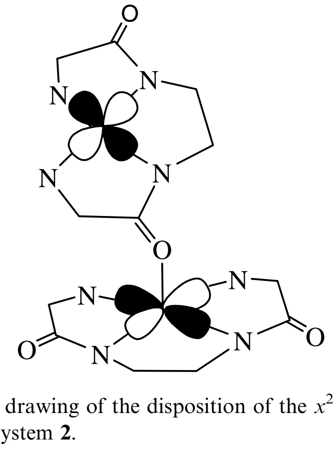

Fig. 6. Schematic drawing of the disposition of the $x^2 - y^2$ orbital in the one-dimensional system **2**.

$-600\ \mathrm{cm}^{-1}$ [51,52]. The extent of coupling (J value) has been found to be very sensitive to the geometry around the terminal Cu(II) ions with respect to the central copper(II) ion. For the square-planar, 4-coordinate, or square-based geometries (such as (4 + 1)- or (4 + 2)-coordinate), the magnetic orbitals are predominantly $d_{x^2-y^2}$ in nature. These terminal metal-based magnetic orbitals are approximately coplanar with that of the central ion and have $x^2 - y^2$ symmetry. Thus, the magnetic coupling is well described by the antibonding combination of the $d_{x^2-y^2}$ metallic orbitals with the symmetry-adapted molecular orbitals of the oxamido bridge. However, in case of trigonal bipyramidal geometry for the terminal copper ions, the magnetic orbitals are predominantly d_{z^2} in character; this reduces the effective overlap and the magnitude of the interaction is smaller (lower value of $-J$) [25–27]. Basically, when the magnetic orbitals of the three Cu(II) ions are not coplanar with respect to each other, the J value decreases. The oxamido ligand provides two coplanars NCO bridging motifs, while for compound **1**, only one NCO group bridge the two Cu(II) ions. Therefore, in compound **1**, with only one way for the magnetic exchange, the antiferromagnetic coupling must be smaller than in the oxamide complexes. This agrees nicely with the smaller J value found for **1** ($-110\ \mathrm{cm}^{-1}$) compared to the oxamido bridged complexes.

The solution state magnetic moment were also determined for both complexes using Evans' method [57]. The room temperature magnetic moment (μ_{eff}) for complex **2** in $(CH_3)_2SO$, was found to be 1.85 μ_B which matches very well with the solid state value of 1.90 μ_B. The similarity between the results from the solid and the solution state indicate a similar structure. However, taking into account that at room temperature if the magnetic coupling is small, the values are close to the uncoupled ions; it is, therefore, not possible to be sure if the 1D structure is maintained or if it is a mononuclear structure in the solution. For trinuclear complex **1**, however, a value of 2.68 μ_B/trimer was obtained at room temperature in $(CH_3)_2SO$ or DMF. This value is lower by ~0.3 μ_B/trimer than the solid state value. The difference in the magnetic moment is indicative of some changes in the geometry of the trinuclear complex and indicate that the copper centres are better antiferromagnetically coupled in the solution state at room temperature. This could happen due to a more relaxed geometry around the copper ions allowing better overlap of the metal based magnetic orbitals through ligand based magnetic orbitals.

3.5. EPR spectra

Powder electron paramagnetic resonance spectra (EPR) were recorded at 298, 77 and 4 K for compounds **1** and **2** (Figs. 7, S4 and S5). The trinuclear complex **1**, with an appreciable antiferromagnetic coupling ($J = -110.34$ cm^{-1}), shows a ground state of $S = 1/2$, and a narrow signal ($\Delta H_{\mathrm{p-p}} = 62$ G) centered at $g = 2.08$ was observed in the EPR spectrum at 4 K. The experimentally observed g value of 2.08 in EPR measurement matches very well with the g value (=2.06) obtained after fitting the magnetic data. For one-dimensional compound, **2**, the EPR spectrum at 4 K, shows two superimposed bands at 2.11 and 2.06, with a $\Delta H_{\mathrm{p-p}} = 145$ G (Fig. 7). The two different g values clearly indicate the anisotropy [58] around the copper centre caused due to the coordination of the O-atom of the neighbour molecule, as observed structurally (cf. crystal structure of **2**). The effect of the temperature in the peak-to-peak gap is opposite in both compounds. For compound **1**, a narrowing of the band was observed on cooling, from 190 to 62 G. However, for **2**, a little broadening of the band was observed, from 130 to 145 G. The observed temperature-dependent behaviour for both complexes clearly indicates that they significantly differ with each other and support their opposite magnetic properties (cf. magnetic measurements).

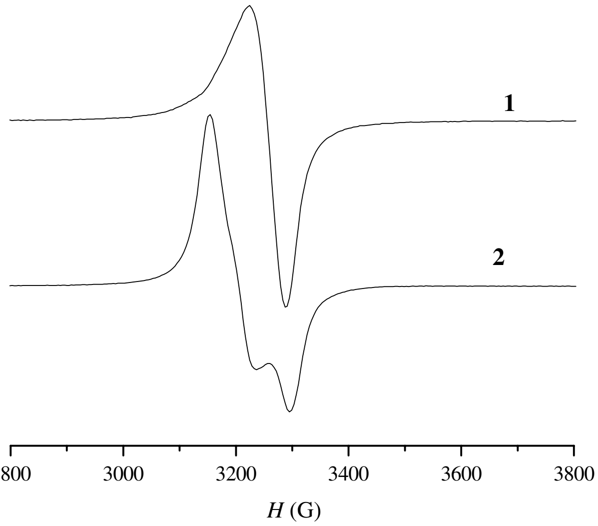

Fig. 7. Powder EPR spectra for compounds **1** and **2** at 4 K.

The EPR spectra were also recorded in the solution state to understand the solution-based geometry and the effect of solvent (CH_3OH and pyridine). For **1**, a broad feature, with the g_{iso} at 2.107 and 2.097 was observed in methanol and pyridine, respectively. In solution, at room temperature there is only one isotropic g value. For complex **2**, a four lines signal was observed in methanol or pyridine at room temperature. This feature is characteristic of the hyperfine coupling with the nuclear spin of the Cu ($I = 3/2$) and typically observed for a tetragonal copper ion in solution [58]. The g_{iso} was observed at ~2.12 with the $A(\mathrm{Cu})_{\mathrm{iso}}$ value of 106 G.

3.6. Absorption spectra

The electronic spectra of both complexes were recorded in the solid state (dispersed in mineral oil) as well as in solutions (CH_3OH, CH_3CN, and pyridine) to gain insight into the coordination geometry around the copper ion (Figs. S6 and S7). The solid state spectrum of **1** displays a broad band in the visible region at 655 with a low energy shoulder at ~850 nm, suggestive of a square-pyramidal geometry [59,60]. A less clear feature was also observed at ~515 nm which we assign due to the square-planar Cu(II) ion. This corroborate the findings from the crystal structure of **1** that clearly show that terminal copper ions are square-planar while the central ion is square-pyramidal. In CH_3OH or CH_3CN, a main peak was observed at 625 nm while a less intense peak at ~515 nm was also noticed. We tentatively assign the former from the square-pyramidal ion (central copper) while the later due to the square-planar ion (terminal coppers). For **2**, a broad band at 590 nm with a weak shoulder at ~760 nm was displayed in the solid state spectrum. These features clearly support a 5-coordinate geometry around the Cu(II) ion [59,60] as seen in the crystal structure of **2**. However, a shift in the λ_{max} was noticed when the spectra were recorded in various solvents; the λ_{max} changed from 530 in CH_3CN to 548 in MeOH to 555 nm in pyridine. This experiment strongly suggests that the axial position(s) occupied by the O_{amide} in the solid state (as seen in the crystal structure) are displaced by the solvent molecule(s) when the spectrum is recorded in the solution state.

4. Conclusions

The present work show interesting coordination behaviour of the amide-based ligands towards copper(II) ion. The backbone flexibility of the ligand $[L^1]^{2-}$, resulted in the flipping of one of the arm to accommodate the second copper ion; this generates the trinuclear complex, $[Cu_3(L^1)_2(Cl)_2(H_2O)]$ **1**. This trinuclear complex belongs to a rare group of complexes where both amidate-N and amidate-O participate in the coordination [31,32]. The ligand $[L^2]^{2-}$, incorporating the rigid *o*-phenylene backbone affords a simple mononuclear complex. The substituted methyl groups restricted the coordination of any additional axial ligand. However, the molecular basal plane tilt in a unique way to allow the coordination of the neighbouring amidate-O to the Cu(II) centre [53,54]. This generates a zig-zag one-dimensional chain, $[Cu(L^2)]_n$ **2**. Both complexes, **1** and **2** have *NCO* bridge between the copper ions and show interesting but contrast magnetic properties. The **1** shows moderately strong antiferromagnetic coupling ($J = \sim -110\ cm^{-1}$). The moderate nature of antiferromagnetic coupling in **1** is due to the availability of only one magnetic exchange pathway (*NCO* bridge) between the copper ions compared to two in the oxamido-bridged systems. Whereas **2** shows a weak ferromagnetic interaction ($J = \sim +3\ cm^{-1}$) due to the accidental orthogonality of the magnetic orbitals from two copper containing basal planes.

Acknowledgements

R.G. thanks University Grant Commission (UGC), Delhi, and Department of Science & Technology (DST), New Delhi for the generous financial support, and DST funded single crystal facility at IIT – Delhi for the data collection of complex **2**. M.C. thanks Ministerio de Educacion y Ciencia for financial support (CTQ2006 – 01759/BQU). J.S. thanks CSIR – UGC for the JRF fellowship.

Appendix A. Supplementary material

CCDC 634199 and 634200 contain the supplementary crystallographic data for **1** and **2**. These data can be obtained free of charge via http://www.ccdc.cam.ac.uk/conts/retrieving.html, or from the Cambridge Crystallographic Data Centre, 12 Union Road, Cambridge CB2 1EZ, UK; fax: (+44) 1223-336-033; or e-mail: deposit@ccdc.cam.ac.uk. Supplementary data associated with this article can be found, in the online version, at doi:10.1016/j.poly.2007.04.021.

References

[1] P.V. Rao, R.H. Holm, Chem. Rev. 104 (2004) 527.
[2] E.I. Solomon, R.K. Szilagyi, S.D. George, L. Basumallick, Chem. Rev. 104 (2004) 419.
[3] M.L. Alvarez, J.Y. Ai, W. Zumft, J. Sanders-Loehr, D.M. Dooley, J. Am. Chem. Soc. 123 (2001) 576.
[4] S. Suzuki, K. Kataoka, K. Yamaguchi, Acc. Chem. Res. 33 (2000) 728.
[5] R.L. Lieberman, D.B. Shrestha, P.E. Doan, B.M. Hoffman, T.L. Stammler, A.C. Rosenzweig, Proc. Natl. Acad. Sci. USA 100 (2003) 3820.
[6] K. Brown, K. Djinovic-Carugo, T. Haltia, I. Cabrito, M. Saraste, J.J.G. Moura, I. Moura, M. Tegoni, C. Cambillau, J. Biol. Chem. 275 (2000) 41133.
[7] K. Brown, M. Tegoni, M. Prudencio, A.S. Pereira, S. Besson, J.J.G. Moura, I. Moura, C. Cambillau, Nat. Struct. Biol. 7 (2000) 191.
[8] B.T. Rasmussen, B.C. Berks, J. Sanders-Loehr, D.M. Dooley, W.G. Zumft, A.J. Thomson, Biochemistry 39 (2000) 12753.
[9] P. Chen, I. Cabrito, J.J.G. Moura, I. Moura, E.I. Solomon, J. Am. Chem. Soc. 124 (2002) 10497.
[10] R.L. Lieberman, A.C. Rosenzweig, Nature 434 (2005) 177.
[11] R.L. Lieberman, K.C. Kondapalli, D.P. Shrestha, A.S. Hakemian, S.M. Smith, J. Telser, J. Kuzelka, R. Gupta, A.S. Borovik, S.J. Lippard, B.M. Hoffman, A.C. Rosenzweig, T.L. Stemmler, Inorg. Chem. 45 (2006) 8372.
[12] M. Melnik, Coord. Chem. Rev. 42 (1982) 259.
[13] D.J. Hodgson, in: S.J. Lippard (Ed.), Progress in Inorganic Chemistry, vol. 19, Wiley, New York, 1975, p. 173.
[14] M. Kato, Y. Muto, Coord. Chem. Rev. 92 (1988) 45.
[15] L. Merz, W. Haase, J. Chem. Soc., Dalton Trans. (1980) 875.
[16] M. Handa, N. Koga, S. Kida, Bull. Chem. Soc. Jpn. 61 (1988) 3853.
[17] R. Gupta, R. Hotchandani, R. Mukherjee, Polyhedron 19 (2000) 1429.
[18] R. Gupta, S. Mukherjee, R. Mukherjee, J. Chem. Soc., Dalton Trans. (1999) 4025.
[19] L.K. Thompson, S.K. Mandal, S.S. Tandon, J.N. Bridson, M.K. Park, Inorg. Chem. 35 (1996) 3117.
[20] S.S. Tandon, L.K. Thompson, J.N. Bridson, V. McKee, A.J. Downard, Inorg. Chem. 31 (1992) 4635.
[21] K. Nonoyama, H. Ojima, K. Ohki, N. Nonoyama, Inorg. Chim. Acta 41 (1980) 155.
[22] N.F. Curtis, I.R.N. McCormick, T.N. Waters, J. Chem. Soc., Dalton Trans. (1973) 1537.
[23] D.M. Duggan, D.N. Hendrickson, Inorg. Chem. 12 (1973) 2422.
[24] Y. Journaux, J. Sletten, O. Kahn, Inorg. Chem. 25 (1986) 439.

[25] A. Garcia, R. Costa, J. Ribas, Inorg. Chim. Acta 168 (1990) 249.

[26] R. Costa, A. Garcia, J. Ribas, T. Mallah, Y. Journaux, J. Sletten, X. Solans, V. Rodriguez, Inorg. Chem. 32 (1993) 3733.

[27] R. Costa, A. Garcia, R. Sanchez, J. Ribas, X. Solans, V. Rodriguez, Polyhedron 12 (1993) 2697.

[28] R. Veit, J.-J. Girerd, O. Kahn, F. Robert, Y. Jeannin, Inorg. Chem. 25 (1986) 4175.

[29] J.-J. Girerd, S. Jeannin, Y. Jeannin, O. Kahn, Inorg. Chem. 17 (1978) 3034.

[30] R. Veit, J.-J. Girerd, O. Kahn, F. Robert, Y. Jeannin, N. El Murr, Inorg. Chem. 23 (1984) 4448.

[31] U.P. Chaudhuri, L.R. Whiteaker, L. Yang, R.P. Houser, Dalton Trans. (2006) 1902.

[32] A. Mondal, Y. Li, M.A. Khan, J.H. Ross Jr., R.P. Houser, Inorg. Chem. 43 (2004) 7075.

[33] A. Davison, A.G. Jones, C. Orvig, M. Sohn, Inorg. Chem. 20 (1981) 1629.

[34] H.-J. Krugar, G. Peng, R.H. Holm, Inorg. Chem. 30 (1991) 734.

[35] Bruker Analytical X-ray System, SMART: Bruker Molecular Analysis Research Tool, Version 5.0 618, 2000.

[36] Bruker Analytical X-ray System, SAINT-NT, Version 6.10, 2000.

[37] G. Cascarano, L. Favia, C. Giacovazzo, J. Appl. Crystallogr. 25 (1992) 310.

[38] G.M. Sheldrick, SHELXL-97: Program for Crystal Structure Refinement, University of Göttingen, Göttingen, Germany, 1997.

[39] L.J. Farrugia, WINGX Version 1.64, An Integrated System of Windows Programs for the Solution, Refinement and Analysis of Single-Crystal X-ray Diffraction Data, Department of Chemistry, University of Glasgow, Glasgow, UK, 2003.

[40] K. Nakamoto, Infrared and Raman Spectra of Inorganic and Coordination Compounds, Wiley, 1986.

[41] W.J. Geary, Coord. Chem. Rev. 7 (1971) 81.

[42] A.W. Addition, T.N. Rao, J. Reedijk, J. van Rijn, G.C. Verschoor, J. Chem. Soc., Dalton Trans. (1984) 1349.

[43] F.S. Stephens, R.S. Vagg, Inorg. Chim. Acta 88 (1984) 7.

[44] F.S. Stephens, R.S. Vagg, Inorg. Chim. Acta 57 (1982) 43.

[45] M. Mulqi, F.S. Stephens, R.S. Vagg, Inorg. Chim. Acta 52 (1981) 177.

[46] F.S. Stephens, R.S. Vagg, Inorg. Chim. Acta 51 (1981) 149.

[47] M. Mulqi, F.S. Stephens, R.S. Vagg, Inorg. Chim. Acta 51 (1981) 9.

[48] J.M. Rowland, M.M. Olmstead, P.K. Mascharak, Inorg. Chem. 39 (2000) 5326.

[49] A. Mondal, E.L. Klein, M.A. Khan, R.P. Houser, Inorg. Chem. 42 (2003) 5462.

[50] M.C.B. de Oliveira, M. Scarpellini, A. Neves, H. Terenzi, A.J. Bortoluzzi, B. Szpoganics, A. Greatti, A.S. Mangrich, E.M. de Souza, P.M. Fernandez, M.R. Soares, Inorg. Chem. 44 (2005) 921.

[51] O. Kahn, Angew. Chem., Int. Ed. Engl. 24 (1985) 834, and references therein.

[52] O. Kahn, Inorg. Chim. Acta 62 (1982) 3, and references therein.

[53] R.L. Chapman, F.S. Stephens, R.S. Vagg, Inorg. Chim. Acta 52 (1981) 169.

[54] R.L. Chapman, F.S. Stephens, R.S. Vagg, Inorg. Chim. Acta 43 (1980) 29.

[55] G.A. Baker, G.S. Rushbreoke, H.E. Gilbert, Phys. Rev. A. 135 (1964) 1272.

[56] D. Gatteschi, L. Pardi, Gazz. Chim. Ital. 123 (1993) 231.

[57] D.F. Evans, J. Chem. Soc. (1959) 2003.

[58] B.J. Hathaway, in: G. Wilkinson, R.D. Gillard, J.A. McCleverty (Eds.), Comprehensive Coordination Chemistry, vol. 5, Pergamon Press, Oxford, 1987, p. 533.

[59] T.K. Lal, R. Gupta, S. Mahapatra, R. Mukherjee, Polyhedron 18 (1999) 1743.

[60] R. Gupta, R. Mukherjee, Polyhedron 19 (2000) 719.